Geophysical Research Letters

RESEARCH LETTER
10.1029/2022GL102655

Reduced Accessible Air–Water Interfacial Area Accelerates PFAS Leaching in Heterogeneous Vadose Zones

Jicai Zeng[1] and **Bo Guo**[1]

[1]Department of Hydrology and Atmospheric Sciences, University of Arizona, Tucson, AZ, USA

Key Points:

- The presence of heterogeneity significantly reduces the accessible air–water interface area in vadose zones
- Reduction of accessible air–water interfacial area amplifies the preferential-flow-induced acceleration of Per- and polyfluoroalkyl substances (PFAS) leaching
- The amplified acceleration is unique for PFAS and is greater for longer chains, drier climates, and more heterogeneous vadose zones

Supporting Information:

Supporting Information may be found in the online version of this article.

Correspondence to:

B. Guo,
boguo@arizona.edu

Citation:

Zeng, J., & Guo, B. (2023). Reduced accessible air–water interfacial area accelerates PFAS leaching in heterogeneous vadose zones. *Geophysical Research Letters*, *50*, e2022GL102655. https://doi.org/10.1029/2022GL102655

Received 3 JAN 2023
Accepted 10 APR 2023

Author Contributions:

Conceptualization: Bo Guo
Data curation: Jicai Zeng
Formal analysis: Jicai Zeng, Bo Guo
Funding acquisition: Bo Guo
Investigation: Jicai Zeng
Methodology: Jicai Zeng, Bo Guo
Project Administration: Bo Guo
Resources: Bo Guo
Software: Jicai Zeng, Bo Guo
Supervision: Bo Guo
Visualization: Jicai Zeng
Writing – original draft: Jicai Zeng
Writing – review & editing: Bo Guo

Abstract Per- and polyfluoroalkyl substances (PFAS) are surface-active contaminants experiencing strong retention in vadose zones due to adsorption at air–water and solid–water interfaces. Leaching of PFAS through vadose zones poses great risks of groundwater contamination. Prior PFAS transport studies have focused on homogenous or layered vadose zones that significantly underrepresented the impact of preferential flow caused by soil heterogeneities—a primary factor known to dominantly control the subsurface transport of many contaminants. We conduct numerical simulations to investigate the impact of preferential flow on PFAS leaching in stochastically generated heterogeneous vadose zones. The simulations show that while shorter-chain PFAS experience accelerated leaching similar to non-surfactant solutes, the accelerated leaching of more surface-active longer-chain PFAS is uniquely amplified by 1.1–4.5 times due to reduced accessible air–water interfacial areas along preferential flow pathways. Our study highlights the criticality of characterizing soil heterogeneities for accurately predicting the leaching of long-chain PFAS in vadose zones.

Plain Language Summary Per- and polyfluoroalkyl substances (PFAS) are a group of emerging contaminants used in many industrial and domestic applications. A growing body of field investigations have shown that PFAS are widespread in the environment. Notably, soils above the groundwater table at many contamination sites serve as significant PFAS reservoirs. PFAS are active at interfaces and tend to accumulate at air–water and solid–water interfaces. This surface activity has led to the strong retention of PFAS in shallow soils (especially the more surface-active PFAS with longer carbon chains). However, field observations have shown that a small fraction of longer-chain PFAS has migrated to deep soils at many contamination sites—in contrast to prior model predictions that underrepresented subsurface heterogeneities. We conduct systematic numerical experiments to test the hypothesis that subsurface heterogeneities accelerate the migration of PFAS in soils. We demonstrate that the heterogeneity-generated preferential flow reduces the air–water interfacial area accessible by PFAS. The accelerated migration is unique to PFAS and is much stronger for longer-chain than that for shorter-chain PFAS. Overall, the present study suggests that characterizing and representing soil heterogeneities are critical for determining the accessible air–water interfacial area and accurately quantifying PFAS contamination risks of groundwater.

1. Introduction

Large-scale manufacturing and wide use of Per- and polyfluoroalkyl substances (PFAS) have led to ubiquitous contamination of surface water, soils, sediments, and groundwater (e.g., Brusseau et al., 2020; Johnson et al., 2022). In particular, field investigations have shown that significant amounts of PFAS have accumulated in the vadose zone. Most PFAS are surfactants and experience strong retention in the vadose zone due to adsorption at air–water and solid–water interfaces. While shorter-chain PFAS appear to be more mobile and are present in deep vadose zones and groundwater, longer-chain PFAS are much more strongly retained and primarily remain in the shallow vadose zone even several decades after the contamination events stopped (e.g., Brusseau et al., 2020; Gnesda et al., 2022; Guo et al., 2020, 2022; Silva et al., 2020; Zeng et al., 2021). However, field data have also demonstrated that longer-chain PFAS do migrate downward to groundwater at some sites, even tens to a hundred meters below the land surface (e.g., AFW, 2019; Dauchy et al., 2019). Understanding what factors control the long-term leaching of PFAS in the vadose zone and reconciling the conflicting observations are therefore critical for assessing risks and mitigating groundwater contamination.

It is widely known that subsurface heterogeneities, such as the presence of macropores, fractures, and soil aggregates, cause preferential transport of contaminants and other solutes (e.g., Brusseau & Rao, 1990; Gelhar, 1986; Jones & Wagenet, 1984; Jury & Horton, 2004; Kung, 1990a, 1990b; Nielsen et al., 1973). Zeng and Guo (2021)

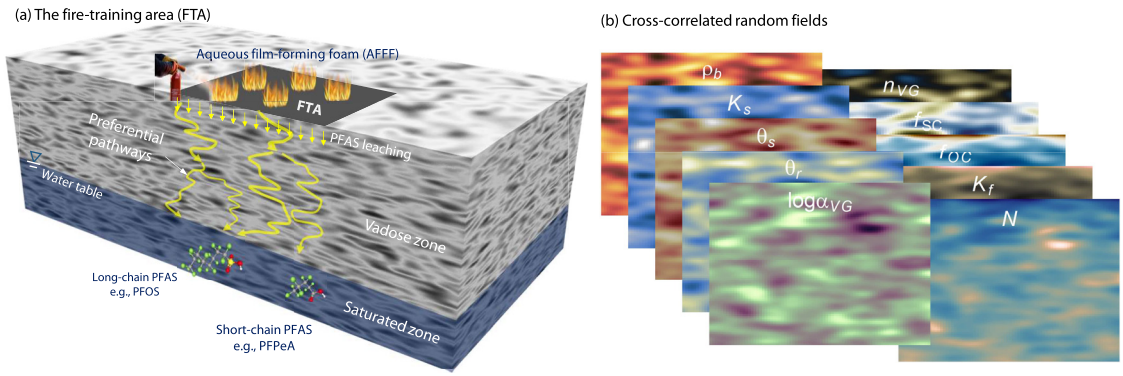

Figure 1. (a) Schematic for Per- and polyfluoroalkyl substances leaching in a heterogeneous vadose zone and (b) example random fields representing the soil heterogeneity.

hypothesized that the migration of longer-chain PFAS to deep vadose zones is caused by heterogeneity-generated preferential flow. Based on preliminary numerical simulations using a few idealized heterogeneity representations including the presence of fractures and lenses of sand and clay, they illustrated that the greater water saturation along heterogeneity-generated preferential flow could destroy air–water interfaces and reduce air–water interfacial adsorption, especially for longer-chain PFAS. While these initial findings provide conceptual and mechanistic insights, the heterogeneities employed in Zeng and Guo (2021) are simple and significantly underrepresent the often-complex field heterogeneities in the subsurface. Whether the amplified preferential leaching of longer-chain PFAS observed in Zeng and Guo (2021) remains a primary factor controlling PFAS leaching in more realistic heterogeneous vadose zones is unknown and needs further investigation.

We present a comprehensive analysis of the impact of preferential flow on the long-term leaching of PFAS in vadose zones under realistic and generalized representations of subsurface heterogeneities. Our objectives are to: (a) quantify to what extent preferential flow reduces the amount of air–water interfacial area in the vadose zone accessible by PFAS, and (b) identify and analyze the primary factors controlling the reduction of accessible air–water interfacial area and their impact on the long-term PFAS leaching in the vadose zone. We stochastically generate a series of heterogeneous vadose zones using field-determined geostatistical parameters (Russo & Bouton, 1992; Russo et al., 1997). We then conduct multidimensional simulations of PFAS transport to quantify the acceleration of PFAS leaching and estimate the accessible air–water interfacial area in the vadose zone. The mathematical model accounts for a wide range of PFAS-specific flow and transport processes, including transient variably saturated flow, surfactant-induced flow, nonlinear and kinetic adsorption at air–water and solid–water interfaces, advection, and dispersion (Guo et al., 2020; Zeng & Guo, 2021).

2. Modeling Soil Water Flow and PFAS Transport in Heterogeneous Vadose Zones

2.1. Mathematical Model for Soil Water Flow and PFAS Transport

We employ the three-dimensional (3D) Richards equation (sometimes also referred to as Richardson-Richards equation) (Richards, 1931; Richardson, 1921) to simulate soil water flow in the vadose zone. The transport of PFAS is modeled by the 3D advection-dispersion equation coupled with two-domain kinetic adsorption at the air–water and solid–water interfaces described in Guo et al. (2020) and Zeng and Guo (2021). More details about the governing equations, parameterization, and numerical schemes are provided in Section S2 in Supporting Information S1.

2.2. PFAS Leaching in the Vadose Zone

We consider PFAS contamination and subsequent leaching in the vadose zone at a 30 m × 30 m model fire-training area (FTA) site (Figure 1a). 30-minute fire-training sessions are assumed to occur every 10 days and last for 30 years. Each session releases approximately 412.5 L of 1% diluted AFFF solution uniformly to the FTA. Two example PFAS representing longer- and shorter-chain compounds (PFOS and PFPeA) are considered in the

AFFF solution. A non-reactive solute (NRS) is included for comparison. Detailed parameters for the two PFAS and the NRS are presented in Section S2.3.2 in Supporting Information S1.

Our simulations consider a 2D cross-section of the vadose zone beneath the FTA. We stochastically generate heterogeneous vadose zones using the geostatistical distributions of soil hydraulic parameters obtained from undisturbed soils collected at a field site (Fiori & Russo, 2007; Russo & Bouton, 1992; Russo et al., 1997, 2001). The field-determined correlation lengths $(\eta_x, \eta_z) = (80\text{ cm}, 20\text{ cm})$ and coefficients of variances (CV_0) are used as the base case (Table S3 in Supporting Information S1). We then vary the correlation lengths (10-times smaller $(\eta_x, \eta_z) = (8\text{ cm}, 2\text{ cm})$) and coefficients of variance ($CV = 0$, $0.5CV_0$, and $1.25CV_0$; $CV = 0$ indicates a homogeneous vadose zone) to cover different characteristic length scales and strengths of heterogeneity. Additionally, we apply these parameters to three types of vadose zones (i.e., clay loam, loam, and sand). The hydraulic parameters and the methods to generate the stochastic realizations are presented in Section S2.3.1 in Supporting Information S1. These random fields are further correlated to the solid-phase adsorption and are also used to generate heterogeneous distributions of air–water interfacial area (methods in Sections S2.2.2–S2.2.3 in Supporting Information S1). Two climatic conditions (semiarid vs. humid) are used to examine the impact of different climate forcings. The initial and boundary conditions, numerical methods, and other information about the model setup are presented in Section S2.4 in Supporting Information S1.

2.3. Method of Analysis

2.3.1. Quantifying PFAS Retention

We quantify PFAS retention in the vadose zone by examining the laterally averaged aqueous concentration of PFAS at a specific vertical depth L over time, $\overline{C}(t)$. We compare the time at which the centroid of the plume arrives at $z = L$ (i.e., the mean travel time of PFAS, T_1) to a characteristic travel time T_c of an NRS. We define $T_c = L\overline{\theta}/\overline{q}_{in}$, where $\overline{q}_{in}$ is the mean infiltration rate (cm/s) and $\overline{\theta}$ is the mean water content of the domain (cm^3/cm^3).

To compute the travel time of the plume centroid, we define the n-th temporal moment of $\overline{C}(t)$ as (e.g., Valocchi, 1990)

$$M_n = \int_0^\infty t^n \overline{C}(t) dt, \tag{1}$$

The normalized n-th temporal moment can be defined as

$$\mu_n = M_n / M_0. \tag{2}$$

Denoting $t_{0.5}$ as half of the contamination release period ($t_{0.5} = 15$ years for the 30-year active contamination in our study), the time at which the plume centroid arrives at $z = L$ can be computed as

$$T_1 = \mu_1 - t_{0.5}, \tag{3}$$

The ratio between T_1 and T_c represents the retention PFAS experience when migrating from the land surface to $z = L$, which can be considered as an effective retardation factor,

$$R = T_1 / T_c. \tag{4}$$

2.3.2. Acceleration Ratio of PFAS Leaching in Heterogeneous Vadose Zones

To quantify the accelerated leaching of PFAS in our simulations, we introduce the concept of acceleration ratio. We denote the acceleration ratio by β and define it as the ratio between the mean travel time of PFAS in a homogenous vadose zone and that in a heterogeneous vadose zone, which can be related to the retardation factors defined in Equation 4 as

$$\beta = R^{homo} / R^{hetero}, \tag{5}$$

where R^{homo} and R^{hetero} are the effective retardation factors computed from Equation 4 for the homogeneous and heterogeneous vadose zones, respectively.

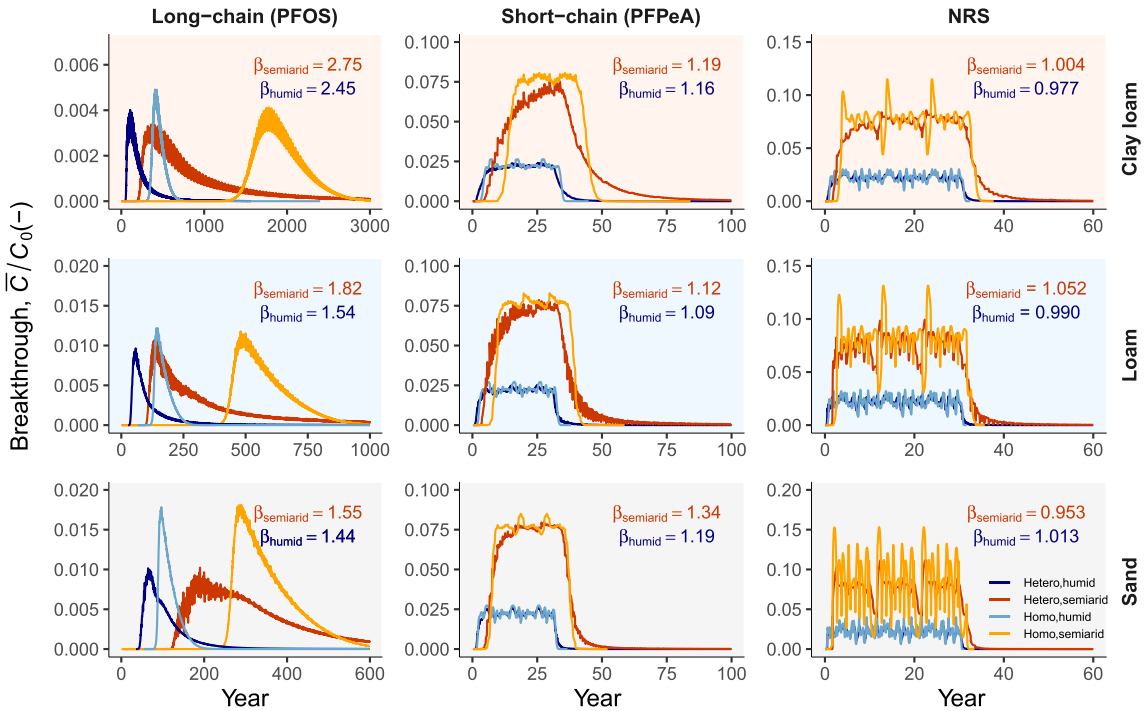

Figure 2. Simulated breakthrough concentrations at a depth of $L = 3.5$ m and computed acceleration ratios (β) for PFOS, PFPeA, and NRS. Three types of heterogeneous vadose zones (clay loam, loam, and sand) and two climatic conditions (semiarid and humid) are considered.

2.3.3. Accessible Air–Water Interfacial Area

The acceleration of PFAS leaching in heterogeneous vadose zones is likely caused by preferential flows reducing the overall air–water interfacial area accessed by PFAS (Zeng & Guo, 2021). To quantify this effect, we determine the mean accessible air–water interfacial area of the domain (denoted as $\overline{A}_{aw}$) in the presence of heterogeneity and compare it to that of a homogenous vadose zone. For each simulation, $\overline{A}_{aw}$ is obtained as follows. We compute the retardation factor using the method introduced in Section 2.3.1 using a separate simulation where we keep everything the same but apply a low release concentration of PFOS (i.e., $C_0 = 0.001$ mg/L such that air–water interfacial adsorption becomes linear) and turn off solid-phase adsorption. More details about this approach to estimate $\overline{A}_{aw}$ is presented in Section S2.5 in Supporting Information S1. Then, assuming equilibrium partitioning of PFAS in the aqueous phase and at air–water interfaces, the effective retardation factor R_{aw} for air–water interfacial adsorption in the domain can be written as $R_{aw} = \overline{A}_{aw}\overline{K}_{aw}/\overline{\theta}$, where $\overline{K}_{aw}$ is the mean air–water interfacial adsorption coefficient that is essentially constant at a low concentration. $\overline{\theta}$ is the mean water content determined from the simulation. Because solid-phase adsorption is turned off, $R_{aw} = R - 1$. $\overline{A}_{aw}$ can then be computed as

$$\overline{A}_{aw} = (R-1)\overline{\theta}/\overline{K}_{aw}. \quad (6)$$

3. Results and Discussion

3.1. Accelerated PFAS Leaching in Heterogeneous Vadose Zones

3.1.1. Breakthrough Concentration and Acceleration Ratio of Leaching

The breakthrough concentration (averaged laterally at $L = 3.5$ m below the land surface) and the computed acceleration ratio (β) for PFOS, PFPeA, and NRS are presented in Figure 2. For all three vadose-zone types, a base heterogeneity case and a homogenous case under semiarid and humid climatic conditions are shown for comparison. C_0 is the concentration in the 1% diluted AFFF solution released to the land surface. Acceleration ratios computed for a broader range of conditions are presented in Table S5 in Supporting Information S1.

As expected, heterogeneity accelerates the leaching of PFAS in the vadose zone, but the acceleration is much more amplified for PFOS than for PFPeA. Conversely, heterogeneity leads to almost negligible acceleration

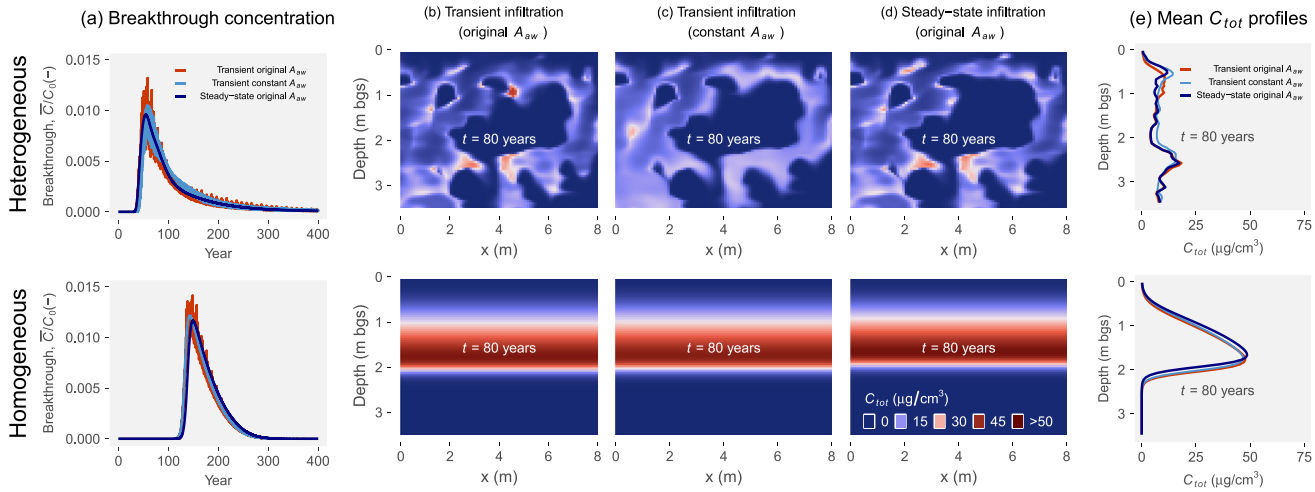

Figure 3. Comparisons between the original transient simulations (with spatially and temporally varying A_{aw} computed live), the constant-A_{aw} transient simulations, and the simulations employing a steady-state infiltration rate. C_{tot} in (b–e) is the total concentration combining mass in the aqueous phase, and air–water and solid–water interfaces.

of NRS ($\beta \approx 1$). In some cases, β is even slightly smaller than 1 because of the long-tailing effects caused by mass-transfer limitations in the lower-permeability zones. Overall, the results suggest that the acceleration ratio is a function of PFAS chain length, soil texture, heterogeneity, and climatic conditions. Among the three types of vadose zones, heterogeneity leads to greater acceleration in the vadose zone with finer-grain soils (clay loam > loam > sand). Conversely, the breakthrough concentrations of NRS among the three vadose-zone types are similar and correlate with the infiltration rates due to their much smaller mean travel times. Stronger heterogeneity (i.e., greater CV) and drier climate also enhance the acceleration. The mechanisms governing the above observations are discussed in Section 3.1.3.

3.1.2. Accessible Air–Water Interfacial Area

Consistent with the acceleration ratios presented in Section 3.1.1, the accessible air–water interfacial area ($\overline{A}_{aw}$) computed from Equation 6 decreases significantly when the vadose zone is heterogeneous (Table S6 in Supporting Information S1). For example, in the base heterogeneity case, $\overline{A}_{aw}$ of the clay-loam vadose zone (humid climate) decreases by 65% from 1,881 to 659 (cm^2/cm^3). Stronger heterogeneity (i.e., greater CV) leads to a greater reduction in $\overline{A}_{aw}$. Additionally, $\overline{A}_{aw}$ also depends on the scale of the heterogeneity (i.e., the correlation length)—$\overline{A}_{aw}$ is generally smaller for $(\eta_x, \eta_z) = (8\text{ cm}, 2\text{ cm})$ than that for $(\eta_x, \eta_z) = (80\text{ cm}, 20\text{ cm})$, which suggests the importance of characterizing heterogeneities at different spatial scales. The mechanisms for the reduced $\overline{A}_{aw}$ are discussed in Section 3.1.3.

An interesting question is whether $\overline{A}_{aw}$ can be applied as a constant air–water interfacial area to the entire domain to effectively predict PFAS leaching in heterogeneous vadose zones. If this is possible, our approach may provide a means to upscale air–water interfacial areas at the field scale. To answer this question, we re-conduct the simulations for PFOS using a constant air–water interfacial area throughout the domain that equals the $\overline{A}_{aw}$ derived from the original simulation; everything else is kept unchanged. Both the base heterogeneity case and the homogeneous case are examined for comparison.

While the breakthrough curves from the constant-A_{aw} simulations do not capture the high-frequency temporal variations, the overall agreement with the original simulations is excellent (Figure 3a; the results for the loamy vadose zone under humid climate are presented as an example). The cumulative mass discharges from the two simulations also agree very well (Figure S9 in Supporting Information S1). The good agreement is further confirmed by the snapshots of the PFOS concentration in space (Figures 3b and 3c) and the mean vertical concentration profiles (Figure 3e) at $t = 80$ years. The constant-A_{aw} approach also works well for the homogeneous case (second row of Figure 3). Between the heterogeneous and homogeneous cases, the front of the PFOS plume in the heterogeneous case migrates much faster due to accelerated leaching, and the mean vertical concentration profile is clearly multimodal (Figure 3e, row 1). The excellent match between the constant-A_{aw} and the

original simulations is surprising, given that the original simulations involve strong dynamics in the air–water interfacial area both temporally and spatially.

A closer inspection reveals that the transients of rainfall infiltration have led to both temporal and spatial variations in the water saturation and air–water interfacial area across the entire vertical depth (see Figures S21 and S22 in Supporting Information S1). For example, the temporal variation of laterally averaged A_{aw} profiles in the preferential pathways of the heterogeneous loamy vadose zone is up to ±50%. To further investigate the impact of transient infiltration, we conduct simulations using a constant infiltration rate that equals the mean net infiltration from the original simulations. All other parameters and conditions are kept the same. The simulated breakthrough concentrations (Figure 3a) and spatial mass distributions are almost identical to those from the original transient simulations (Figure 3b vs. 3d). This suggests that assuming steady-state water flow (i.e., simulated using the long-term averaged net infiltration rate) appears to be adequate for modeling long-term PFAS leaching even for strongly heterogeneous vadose zones. However, we note that this finding is based on the range of conditions and heterogeneities modeled in the present study. Further investigations especially direct field observations are needed to generalize this model-based analysis.

3.1.3. Mechanisms Underlying the Reduced Accessible Air–Water Interfacial Area and Accelerated Leaching

Because preferential flow pathways in vadose zones often have higher S_w (e.g., Kung, 1990a, 1990b) and greater S_w destroys air–water interfaces, it is likely that the reduced accessible $\overline{A}_{aw}$ is caused by heterogeneity-induced preferential flow pathways (Zeng & Guo, 2021). Here we conduct additional analyses to quantify the degree to which preferential flow pathways are responsible for the reduced $\overline{A}_{aw}$ and the accelerated leaching.

For each simulation, we obtain the air–water interfacial area and water saturation for each numerical cell at every time step and plot them on the A_{aw}–S_w diagram. For each (A_{aw}, S_w) pair, we also obtain the corresponding Darcy water flux and use the size of the circle to denote its magnitude. Denoting $q_{max} = max(|\boldsymbol{q}|)$ as the maximum Darcy flux in space and time, ranking the Darcy water flux identifies the (A_{aw}, S_w) points that belong to the preferential flow pathways: we define $0.1q_{max}$ to q_{max} as the preferential flow pathways, $<0.01q_{max}$ as the slow flow zone, and between $0.01q_{max}$ and $0.1q_{max}$ as the intermediate flow zone. The threshold of $0.1q_{max}$ is selected such that the "preferential flow" numerical cells form a connected network from the land surface to the bottom of the domain (Figure 4a). The simulated (A_{aw}, S_w) pairs for the homogeneous vadose zone are included for comparison. We have also included A_{aw} as a function of S_w for three reference soil types (i.e., sand, clay loam, and clay). The analyses below use the simulations for the clay-loam vadose zone under humid climate as an example. The results for the other cases are presented in Figures S11–S15 in Supporting Information S1.

The location of a (A_{aw}, S_w) pair relative to the curves of the three reference soils provides a means to identify the soil type of the numerical cell. Consistent with prior studies of preferential flow (e.g., Jury & Horton, 2004; Kung, 1990a, 1990b), most of the numerical cells along the preferential flow pathways appear to have finer-grain soil types, but their A_{aw} is relatively small due to high S_w (Zeng & Guo, 2021). The sandy regions also have small A_{aw}, but their S_w and unsaturated hydraulic conductivity (K) are too small to allow water and PFAS to go through. These observations concur with the probability distributions of θ_s, θ_r, α_{VG}, n_{VG}, K_s, K, S_w, and A_{aw} for the numerical cells in the two flow zones (Figures 4c1–4c8), which consistently show that the majority of the preferential flow pathways are composed of finer-grain soils. The representative A_{aw} (~190 cm^2/cm^3) of the preferential flow pathways is much smaller than that in the slow flow zone (~400–741 cm^2/cm^3) and the homogeneous vadose zone (~1,767 cm^2/cm^3, Figure 4c8). Finally, because the $A_{aw}(S_w)$ function for each soil becomes more nonlinear at lower S_w, preferential flow pathways will lead to a greater reduction in $\overline{A}_{aw}$ under a drier climate. This is likely why the acceleration ratio and reduction of $\overline{A}_{aw}$ in Sections 3.1.1 and 3.1.2 are greater for the semiarid climate than that for the humid climate.

We plot β versus $\overline{A}_{aw}^{homo}/\overline{A}_{aw}^{hetero}$ for PFOS, PFPeA, and NRS (Figure S16 in Supporting Information S1) to further illustrate that the accelerated leaching due to the reduced $\overline{A}_{aw}$ is a phenomenon unique to the more surface-active longer-chain PFAS. Figure S16 in Supporting Information S1 shows that, for PFPeA and NRS, β remains mostly unchanged as $\overline{A}_{aw}^{homo}/\overline{A}_{aw}^{hetero}$ increases. Conversely, for PFOS, β increases almost linearly with $\overline{A}_{aw}^{homo}/\overline{A}_{aw}^{hetero}$. This suggests that the amplified acceleration for more surface-active PFAS is mainly attributed to the reduced $\overline{A}_{aw}$. However, it is interesting that the slope of β starts to decrease for greater $\overline{A}_{aw}^{homo}/\overline{A}_{aw}^{hetero}$. A closer inspection reveals

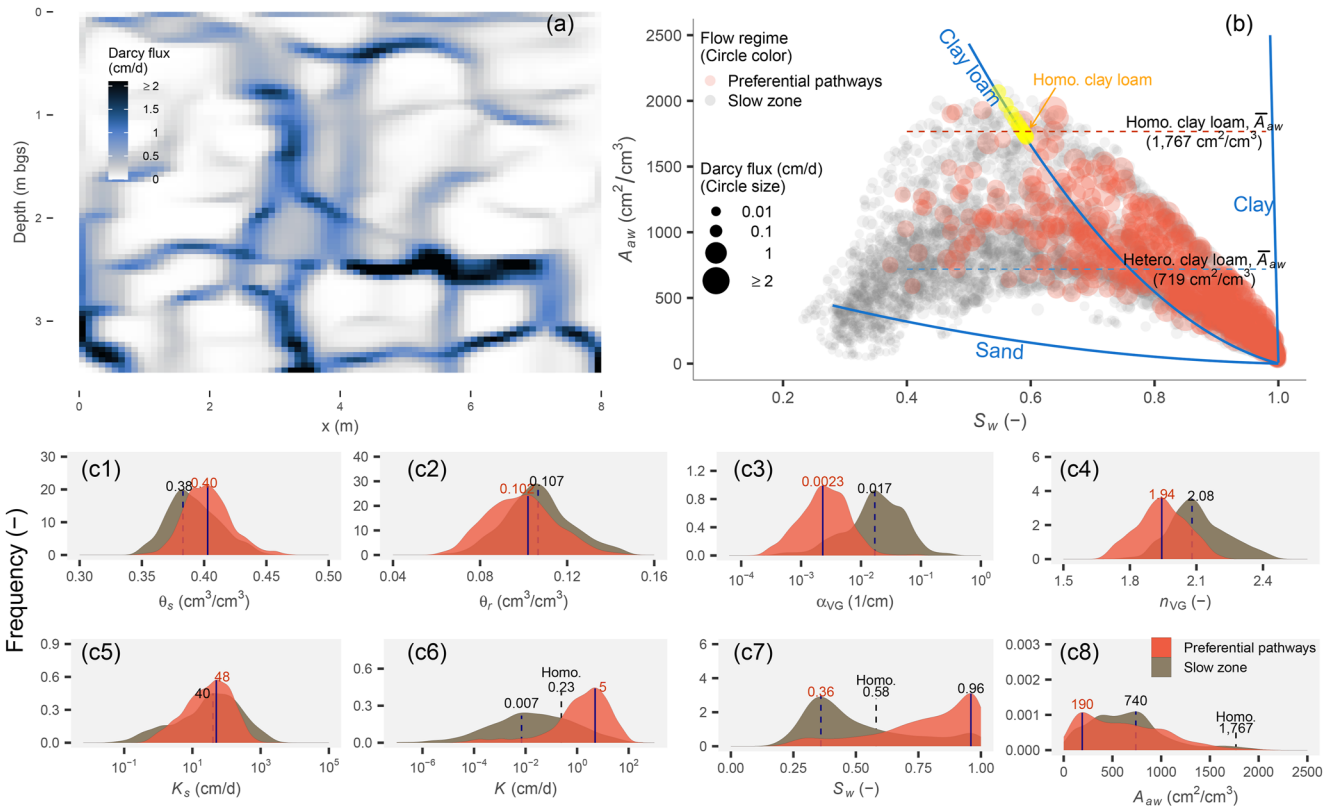

Figure 4. (a) Spatial distribution of the Darcy flux (averaged in time) for identifying preferential flow pathways. (b) A_{aw}–S_w diagram for each numerical cell from the entire simulation (red, gray, and yellow circles, respectively, indicate the preferential flow pathways, slow flow zones, and numerical cells in the homogeneous case; the three solid A_{aw}–S_w curves correspond to the reference soils: clay, clay loam, and sand. (c1–c8) Probability distributions of θ_s, θ_r, α_{VG}, n_{VG}, K_s, K, S_w, and A_{aw}. The maximum Darcy flux in the domain (q_{max}) is 3.47 cm/d.

that it is caused by greater solid-phase adsorption in the finer soil textures along the preferential pathways. This indicates that the solid-phase adsorption being correlated to soil heterogeneity can work against the amplified accelerated leaching by the reduced air–water interfacial adsorption along the preferential flow pathways under certain heterogeneous conditions. To further investigate this aspect, we compare the simulations with and without correlating the solid-phase adsorption and soil heterogeneity (Section S4.2 in Supporting Information S1). The results suggest a limited impact on the accelerated leaching for the simulations examined in the present study. However, we note that the correlation between solid-phase adsorption and soil heterogeneity may become a more important factor in vadose zones with much stronger solid-phase adsorption capacities.

3.2. Comments on Additional Factors

In a prior study, Zeng et al. (2021) reported that kinetic solid-phase adsorption has a minimum impact on PFAS leaching in homogeneous vadose zones. Our results suggest that PFAS leaching remains insensitive to kinetic solid-phase adsorption even in the presence of strongly transient infiltration and preferential flow in highly heterogeneous vadose zones (Figure S17 in Supporting Information S1). However, the present study used the first-order rate constants determined from soil samples collected at one particular AFFF-impacted site (Schaefer et al., 2021). Generalization to other contamination sites will require the use of site-specific parameters for kinetic solid-phase adsorption/desorption.

Additionally, we have conducted 3D simulations using the same boundary conditions and geostatistical parameters to confirm the validity of 2D cross-sectional representations of a 3D vadose zone used in the present study. The accelerated leaching behavior similar to that in the 2D simulations is observed in the 3D simulations (Figure S24 in Supporting Information S1). Finally, the variations among Monte Carlo simulations are relatively small (Figures S24 and S25 in Supporting Information S1), which indicates that the "single-realization" approach

suggested by prior studies (e.g., Ababou et al., 1988; Polmann et al., 1991; Russo et al., 1994) is valid for the analyses in the present study.

4. Summary and Conclusion

We present a series of multidimensional numerical experiments to examine PFAS leaching in heterogeneous vadose zones. The mathematical model accounts for transient variably saturated flow, surfactant-induced flow, and advective and dispersive transport processes coupled with kinetic and nonlinear adsorption at air–water and solid–water interfaces. The heterogeneous vadose zones are randomly generated using field-determined geostatistical distributions. These random parameter fields are then correlated to the solid-phase adsorption and are also used to generate heterogenous distributions of air–water interfacial area.

The simulations suggest that while the presence of heterogeneity and preferential flow leads to accelerated leaching for all PFAS, the more surface-active long-chain PFOS experiences much stronger acceleration. The amplified acceleration for PFOS is caused by the significantly reduced accessible air–water interfacial area in the preferential flow pathways. In addition to the surface activity of PFAS, the acceleration is more prominent for vadose zones with stronger heterogeneity and under drier climate conditions. Depending on the specific conditions, the leaching of PFOS is accelerated by 1.1–4.5 times for the scenarios examined in the present study.

Our study suggests that it is critical to characterize soil heterogeneities for accurate predictions of PFAS leaching in the vadose zone. Numerical simulations indicate that both smaller- and greater-scale heterogeneities can lead to accelerated leaching of PFAS in the vadose zone, which may explain the leaching of long-chain PFAS to the deep subsurface at some sites despite that the vadose zone is relatively homogeneous in each soil layer (e.g., Dauchy et al., 2019). Finally, the accelerated leaching in heterogeneous vadose zones due to the reduced accessible air–water interfacial area also applies to other surface-active contaminants and particles where accumulations at the air–water interfaces contribute to their retention in the vadose zone (e.g., Abdel-Fattah & El-Genk, 1998; Sharma et al., 2008; Wan & Tokunaga, 2002).

Data Availability Statement

All the datasets used in the present study are included in the paper and its supporting information, tables, and figures. These datasets are also available at https://doi.org/10.5281/zenodo.7699345. The numerical model used to conduct the numerical simulations has been reported previously by Guo et al. (2020) and Zeng and Guo (2021).

Acknowledgments
This work is in part supported by the Environmental Security Technology Certification Program (Project ER21-5041) and the National Science Foundation (2023351 and 2054575). We thank the reviewers for their constructive comments that led to the additional analyses of solid-phase adsorption being correlated to soil textures and Dr. Yonggen Zhang (Tianjin University) for his assistance in applying the pedo-transfer function.

References

Ababou, R., Gelhar, L. W., & McLaughlin, D. (1988). Three-dimensional flow in random porous media Retrieved from https://www.nrc.gov/docs/ML0330/ML033070298.pdf

Abdel-Fattah, A. I., & El-Genk, M. S. (1998). On colloidal particle sorption onto a stagnant air–water interface. *Advances in Colloid and Interface Science*, *78*(3), 237–266. https://doi.org/10.1016/S0001-8686(98)00066-9

AFW (Amec Foster Wheeler Environment & Infrastructure, Inc.). (2019). *Final site inspection of aqueous film forming foam (AFFF) Release areas, environmental programs worldwide, installation-specific work plan*. Davis-Monthan Air Force Base.

Brusseau, M. L., Anderson, R. H., & Guo, B. (2020). PFAS concentrations in soils: Background levels versus contaminated sites. *Science of the Total Environment*, *740*, 140017. https://doi.org/10.1016/j.scitotenv.2020.140017

Brusseau, M. L., & Rao, P. S. C. (1990). Modeling solute transport in structured soils: A review. *Geoderma*, *46*(1–3), 169–192. https://doi.org/10.1016/0016-7061(90)90014-Z

Dauchy, X., Boiteux, V., Colin, A., Hémard, J., Bach, C., Rosin, C., & Munoz, J. F. (2019). Deep seepage of per-and polyfluoroalkyl substances through the soil of a firefighter training site and subsequent groundwater contamination. *Chemosphere*, *214*, 729–737. https://doi.org/10.1016/j.chemosphere.2018.10.003

Fiori, A., & Russo, D. (2007). Numerical analyses of subsurface flow in a steep hillslope under rainfall: The role of the spatial heterogeneity of the formation hydraulic properties. *Water Resources Research*, *43*(7), W07445. https://doi.org/10.1029/2006WR005365

Gelhar, L. W. (1986). Stochastic subsurface hydrology from theory to applications. *Water Resources Research*, *22*(9S), 135S–145S. https://doi.org/10.1029/WR022i09Sp0135S

Gnesda, W. R., Draxler, E. F., Tinjum, J., & Zahasky, C. (2022). Adsorption of PFAAs in the vadose zone and implications for long-term groundwater contamination. *Environmental Science & Technology*, *56*(23), 16748–16758. https://doi.org/10.1021/acs.est.2c03962

Guo, B., Zeng, J., & Brusseau, M. L. (2020). A mathematical model for the release, transport, and retention of per-and polyfluoroalkyl substances (PFAS) in the vadose zone. *Water Resources Research*, *56*(2), e2019WR026667. https://doi.org/10.1029/2019WR026667

Guo, B., Zeng, J., Brusseau, M. L., & Zhang, Y. (2022). A screening model for quantifying PFAS leaching in the vadose zone and mass discharge to groundwater. *Advances in Water Resources*, *160*, 104102. https://doi.org/10.1016/j.advwatres.2021.104102

Johnson, G. R., Brusseau, M. L., Carroll, K. C., Tick, G. R., & Duncan, C. M. (2022). Global distributions, source-type dependencies, and concentration ranges of per-and polyfluoroalkyl substances in groundwater. *Science of the Total Environment*, *841*, 156602. https://doi.org/10.1016/j.scitotenv.2022.156602

Jones, A. J., & Wagenet, R. J. (1984). In situ estimation of hydraulic conductivity using simplified methods. *Water Resources Research*, *20*(11), 1620–1626. https://doi.org/10.1029/WR020i011p01620
Jury, W. A., & Horton, R. (2004). *Soil physics*. John Wiley & Sons.
Kung, K. J. S. (1990a). Preferential flow in a sandy vadose zone: 1. Field observation. *Geoderma*, *46*(1–3), 51–58. https://doi.org/10.1016/0016-7061(90)90006-U
Kung, K. J. S. (1990b). Preferential flow in a sandy vadose zone: 2. Mechanism and implications. *Geoderma*, *46*(1–3), 59–71. https://doi.org/10.1016/0016-7061(90)90007-V
Nielsen, D. R., Biggar, J. W., & Erh, K. T. (1973). Spatial variability of field-measured soil-water properties. https://doi.org/10.3733/hilg.v42n07p215
Polmann, D. J., McLaughlin, D., Luis, S., Gelhar, L. W., & Ababou, R. (1991). Stochastic modeling of large-scale flow in heterogeneous unsaturated soils. *Water Resources Research*, *27*(7), 1447–1458. https://doi.org/10.1029/91WR00762
Richards, L. A. (1931). Capillary conduction of liquids through porous mediums. *Journal of Applied Physics*, *1*(5), 318–333. https://doi.org/10.1063/1.1745010
Richardson, L. F. (1921). *Weather prediction by numerical process*. Cambridge university press.
Russo, D., & Bouton, M. (1992). Statistical analysis of spatial variability in unsaturated flow parameters. *Water Resources Research*, *28*(7), 1911–1925. https://doi.org/10.1029/92WR00669
Russo, D., Russo, I., & Laufer, A. (1997). On the spatial variability of parameters of the unsaturated hydraulic conductivity. *Water Resources Research*, *33*(5), 947–956. https://doi.org/10.1029/96WR03947
Russo, D., Zaidel, J., & Laufer, A. (1994). Stochastic analysis of solute transport in partially saturated heterogeneous soil: 2. Prediction of solute spreading and breakthrough. *Water Resources Research*, *30*(3), 781–790. https://doi.org/10.1029/93WR02883
Sharma, P., Flury, M., & Zhou, J. (2008). Detachment of colloids from a solid surface by a moving air–water interface. *Journal of Colloid and Interface Science*, *326*(1), 143–150. https://doi.org/10.1016/j.jcis.2008.07.030
Silva, J. A. K., Šimůnek, J., & McCray, J. E. (2020). A modified HYDRUS model for simulating PFAS transport in the vadose zone. *Water*, *12*(10), 2758. https://doi.org/10.3390/w12102758
Valocchi, A. J. (1990). Use of temporal moment analysis to study reactive solute transport in aggregated porous media. *Geoderma*, *46*(1–3), 233–247. https://doi.org/10.1016/0016-7061(90)90017-4
Wan, J., & Tokunaga, T. K. (2002). Partitioning of clay colloids at air–water interfaces. *Journal of Colloid and Interface Science*, *247*(1), 54–61. https://doi.org/10.1006/jcis.2001.8132
Zeng, J., Brusseau, M. L., & Guo, B. (2021). Model validation and analyses of parameter sensitivity and uncertainty for modeling long-term retention and leaching of PFAS in the vadose zone. *Journal of Hydrology*, *603*, 127172. https://doi.org/10.1016/j.jhydrol.2021.127172
Zeng, J., & Guo, B. (2021). Multidimensional simulation of PFAS transport and leaching in the vadose zone: Impact of surfactant-induced flow and subsurface heterogeneities. *Advances in Water Resources*, *155*, 104015. https://doi.org/10.1016/j.advwatres.2021.104015

References From the Supporting Information

Adamson, A. W., & Gast, A. P. (1967). *Physical chemistry of surfaces* (Vol. 150, p. 180). Interscience publishers.
Alabert, F. (1987). The practice of fast conditional simulations through the LU decomposition of the covariance matrix. *Mathematical Geology*, *19*(5), 369–386. https://doi.org/10.1007/BF00897191
Anderson, R. H., Feild, J. B., Dieffenbach-Carle, H., Elsharnouby, O., & Krebs, R. K. (2022). Assessment of PFAS in collocated soil and porewater samples at an AFFF-impacted source zone: Field-scale validation of suction lysimeters. *Chemosphere*, *308*, 136247. https://doi.org/10.1016/j.chemosphere.2022.136247
Bear, J. (1988). *Dynamics of fluids in porous media Dover Publications*. Dover Publication, Inc.
Bradford, S. A., & Leij, F. J. (1997). Estimating interfacial areas for multi-fluid soil systems. *Journal of Contaminant Hydrology*, *27*(1–2), 83–105. https://doi.org/10.1016/S0169-7722(96)00048-4
Brusseau, M. L., El Ouni, A., Araujo, J. B., & Zhong, H. (2015). Novel methods for measuring air-water interfacial area in unsaturated porous media. *Chemosphere*, *127*, 208–213. https://doi.org/10.1016/j.chemosphere.2015.01.029
Brusseau, M. L., & Guo, B. (2021). Air-water interfacial areas relevant for transport of per and poly-fluoroalkyl substances. *Water Research*, *207*, 117785. https://doi.org/10.1016/j.watres.2021.117785
Brusseau, M. L., & Guo, B. (2022). PFAS concentrations in soil versus soil porewater: Mass distributions and the impact of adsorption at air-water interfaces. *Chemosphere*, *302*, 134938. https://doi.org/10.1016/j.chemosphere.2022.134938
Brusseau, M. L., Hu, Q., & Srivastava, R. (1997). Using flow interruption to identify factors causing nonideal contaminant transport. *Journal of Contaminant Hydrology*, *24*(3–4), 205–219. https://doi.org/10.1016/S0169-7722(96)00009-5
Brusseau, M. L., Popovicova, J., & Silva, J. A. (1997). Characterizing gas-water interfacial and bulk-water partitioning for gas-phase transport of organic contaminants in unsaturated porous media. *Environmental Science & Technology*, *31*(6), 1645–1649. https://doi.org/10.1021/es960475j
Brusseau, M. L., Peng, S., Schnaar, G., & Murao, A. (2007). Measuring air-water interfacial areas with x-ray microtomography and interfacial partitioning tracer tests. *Environmental Science & Technology*, *41*(6), 1956–1961. https://doi.org/10.1021/es061474m
Brusseau, M. L., & Rao, P. S. C. (1991). Influence of sorbate structure on nonequilibrium sorption of organic compounds. *Environmental Science & Technology*, *25*(8), 1501–1506. https://doi.org/10.1021/es00020a022
Carsel, R. F., & Parrish, R. S. (1988). Developing joint probability distributions of soil water retention characteristics. *Water Resources Research*, *24*(5), 755–769. https://doi.org/10.1029/WR024i005p00755
Celia, M. A., Bouloutas, E. T., & Zarba, R. L. (1990). A general mass-conservative numerical solution for the unsaturated flow equation. *Water Resources Research*, *26*(7), 1483–1496. https://doi.org/10.1029/WR026i007p01483
Chapelle, F. H., Kauffman, L. J., & Widdowson, M. A. (2014). Modeling the effects of naturally occurring carbon on chlorinated ethene transport to a public water supply well. *Groundwater*, *52*(S1), 76–89. https://doi.org/10.1111/gwat.12152
Clark, K. (2016). *AmeriFlux US-Slt Silas Little-New Jersey. Lawrence Berkeley National Lab. (LBNL)*. USDA Forest Service. https://doi.org/10.17190/AMF/1246096
van Genuchten, M. T. (1980). A closed-form equation for predicting the hydraulic conductivity of unsaturated soils. *Soil Science Society of America Journal*, *44*(5), 892–898. https://doi.org/10.2136/sssaj1980.03615995004400050002x
Jiang, H., Guo, B., & Brusseau, M. L. (2020). Pore-scale modeling of fluid-fluid interfacial area in variably saturated porous media containing microscale surface roughness. *Water Resources Research*, *56*(1), e2019WR025876. https://doi.org/10.1029/2019WR025876

Jobbágy, E. G., & Jackson, R. B. (2000). The vertical distribution of soil organic carbon and its relation to climate and vegetation. *Ecological Applications*, *10*(2), 423–436. https://doi.org/10.1890/1051-0761(2000)010[0423:TVDOSO]2.0.CO;2

Kim, H., Rao, P. S. C., & Annable, M. D. (1997). Determination of effective air-water interfacial area in partially saturated porous media using surfactant adsorption. *Water Resources Research*, *33*(12), 2705–2711. https://doi.org/10.1029/97WR02227

Leverett, M. C. (1941). Capillary behavior in porous solids. *OR Transactions*, *142*(1), 152–169. https://doi.org/10.2118/941152-G

MacIntyre, W. G., & Stauffer, T. B. (1989). *Liquid chromatography applications to determination of sorption on aquifer materials* (pp. 38). Air Force Engineering & Services Laboratory. https://doi.org/10.1016/0045-6535(88)90164-6

Millington, R. J., & Quirk, J. P. (1961). Permeability of porous solids. *Transactions of the Faraday Society*, *57*, 1200–1207. https://doi.org/10.1039/TF9615701200

Mishra, S., Parker, J. C., & Singhal, N. (1989). Estimation of soil hydraulic properties and their uncertainty from particle size distribution data. *Journal of Hydrology*, *108*, 1–18. https://doi.org/10.1016/0022-1694(89)90275-8

Morrow, N. R. (1970). Physics and thermodynamics of capillary action in porous media. *Industrial and Engineering Chemistry*, *62*(6), 32–56. https://doi.org/10.1021/ie50726a006

Mualem, Y. (1976). A new model for predicting the hydraulic conductivity of unsaturated porous media. *Water Resources Research*, *12*(3), 513–522. https://doi.org/10.1029/WR012i003p00513

Paviostathis, S. G., & Mathavan, G. N. (1992). Desorption kinetics of selected volatile organic compounds from field contaminated soils. *Environmental Science & Technology*, *26*(2), 532–538. https://doi.org/10.1021/es00027a014

Pebesma, E. J. (2004). Multivariable geostatistics in S: The gstat package. *Computers & Geosciences*, *30*(7), 683–691. https://doi.org/10.1016/j.cageo.2004.03.012

Peng, S., & Brusseau, M. L. (2012). Air-water interfacial area and capillary pressure: Porous-Medium texture effects and an empirical function. *Journal of Hydrologic Engineering*, *17*(7), 829–832. https://doi.org/10.1061/(ASCE)HE.1943-5584.0000515

Quinnan, J., Rossi, M., Curry, P., Lupo, M., Miller, M., Korb, H., et al. (2021). Application of PFAS-mobile lab to support adaptive characterization and flux-based conceptual site models at AFFF releases. *Remediation Journal*, *31*(3), 7–26. https://doi.org/10.1002/rem.21680

Roberts, P. V., Hopkins, G. D., Mackay, D. M., & Semprini, L. (1990). A field evaluation of in-situ biodegradation of chlorinated ethenes: Part I, methodology and field site characterization. *Groundwater*, *28*(4), 591–604. https://doi.org/10.1111/j.1745-6584.1990.tb01716.x

Rosen, M. J., & Kunjappu, J. T. (2012). *Surfactants and interfacial phenomena. Surfactants and interfacial phenomena* (4th ed.). John Wiley & Sons, Inc. https://doi.org/10.1002/9781118228920

Russo, D., & Fiori, A. (2008). Equivalent vadose zone steady state flow: An assessment of its capability to predict transport in a realistic combined vadose zone–groundwater flow system. *Water Resources Research*, *44*(9), W09436. https://doi.org/10.1029/2007WR006170

Russo, D., Zaidel, J., & Laufer, A. (1998). Numerical analysis of flow and transport in a three-dimensional partially saturated heterogeneous soil. *Water Resources Research*, *34*(6), 1451–1468. https://doi.org/10.1029/98WR00435

Russo, D., Zaidel, J., & Laufer, A. (2001). Numerical analysis of flow and transport in variably saturated bimodal heterogeneous porous media. *Water Resources Research*, *37*(8), 2127–2141. https://doi.org/10.1029/2001WR000393

Schaap, M. G., Leij, F. J., & Van Genuchten, M. T. (2001). Rosetta: A computer program for estimating soil hydraulic parameters with hierarchical pedotransfer functions. *Journal of Hydrology*, *251*(3–4), 163–176. https://doi.org/10.1016/S0022-1694(01)00466-8

Schaefer, C., DiCarlo, D., & Blunt, M. (2000). Experimental measurement of air-water interfacial area during gravity drainage and secondary imbibition in porous media. *Water Resources Research*, *36*(4), 885–890. https://doi.org/10.1029/2000WR900007

Schaefer, C. E., Lavorgna, G. M., Lippincott, D. R., Nguyen, D., Christie, E., Shea, S., et al. (2022). A field study to assess the role of air-water interfacial sorption on PFAS leaching in an AFFF source area. *Journal of Contaminant Hydrology*, *248*, 104001. https://doi.org/10.1016/j.jconhyd.2022.104001

Schaefer, C. E., Nguyen, D., Christie, E., Shea, S., Higgins, C. P., & Field, J. A. (2021). Desorption of poly-and perfluoroalkyl substances from soil historically impacted with aqueous film-forming foam. *Journal of Environmental Engineering*, *147*(2), 06020006. https://doi.org/10.1061/(ASCE)EE.1943-7870.0001846

Scott, R. (2016). *AmeriFlux US-Wkg Walnut Gulch Kendall Grasslands. Lawrence Berkeley National Lab. (LBNL)*. AmeriFlux, United States Department of Agriculture. https://doi.org/10.17190/AMF/1246112

Smith, J. E., & Gillham, R. W. (1994). The effect of concentration-dependent surface tension on the flaw of water and transport of dissolved organic compounds: A pressure head-based formulation and numerical model. *Water Resources Research*, *30*(2), 343–354. https://doi.org/10.1029/93WR02745

Vereecken, H., Maes, J., Feyen, J., & Darius, P. (1989). Estimating the soil moisture retention characteristic from texture, bulk density, and carbon content. *Soil Science*, *148*(6), 389–403. https://doi.org/10.1097/00010694-198912000-00001

Wang, G., Allen-King, R. M., Choung, S., Feenstra, S., Watson, R., & Kominek, M. (2013). A practical measurement strategy to estimate nonlinear chlorinated solvent sorption in low foc sediments. *Groundwater Monitoring & Remediation*, *33*(1), 87–96. https://doi.org/10.1111/j.1745-6592.2012.01413.x

Woods, L., Siegrist, R. L., & Crimi, M. (2012). Effects of in situ remediation using oxidants and surfactants on subsurface organic matter and sorption of trichloroethene. *Groundwater Monitoring & Remediation*, *32*(2), 96–105. https://doi.org/10.1111/j.1745-6592.2011.01377.x

Xu, M., & Eckstein, Y. (1995). Use of weighted least-squares method in evaluation of the relationship between dispersivity and field scale. *Ground Water*, *33*(6), 905–908. https://doi.org/10.1111/j.1745-6584.1995.tb00035.x

Zhang, C., Yan, H., Li, F., Hu, X., & Zhou, Q. (2013). Sorption of short-and long-chain perfluoroalkyl surfactants on sewage sludges. *Journal of Hazardous Materials*, *260*, 689–699. https://doi.org/10.1016/j.jhazmat.2013.06.022

Zhang, Y., Schaap, M. G., & Wei, Z. (2020). Development of hierarchical ensemble model and estimates of soil water retention with global coverage. *Geophysical Research Letters*, *47*(15), e2020GL088819. https://doi.org/10.1029/2020GL088819